ACS Catalysis

Research Article

pubs.acs.org/acscatalysis

Theoretical Analysis of Transition-Metal Catalysts for Formic Acid Decomposition

Jong Suk Yoo,[†] Frank Abild-Pedersen,[‡] Jens K. Nørskov,[†,‡] and Felix Studt*[,‡]

[†]Department of Chemical Engineering, Stanford University, Stanford, California 94305, United States

[‡]SUNCAT Center for Interface Science and Catalysis, SLAC National Accelerator Laboratory, 2575 Sand Hill Road, Menlo Park, California 94025, United States

Supporting Information

ABSTRACT: Periodic density functional theory calculations are employed to determine the reaction energetics of formic acid decomposition on Ag, Cu, Pd, Pt, and Rh surfaces. We also extend the study to other transition-metal surfaces by scaling the adsorption energies of the reaction species with two independent descriptors: CO and OH adsorption energies. A microkinetic model is then developed to derive the kinetics of formic acid decomposition from the energy parameters. By incorporating the scaling relations in the microkinetic model, the turnover frequencies for formic acid decomposition over the transition-metal surfaces are described as functions of the two descriptors. The variations in catalytic activity and selectivity from one metal surface to another, which are obtained from the first principles analysis, are in qualitative agreement with those obtained experimentally. The interpolation concept of adsorption energy is finally used to conveniently identify potentially interesting alloy catalysts for formic acid decomposition.

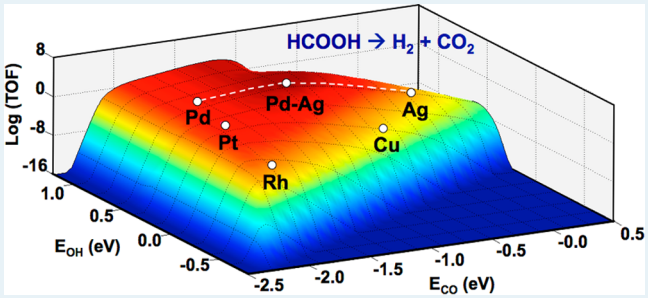

KEYWORDS: *formic acid decomposition, hydrogen storage, hydrogen production, catalyst, density functional theory, scaling relation, microkinetic model, first principles analysis, descriptor based analysis, interpolation*

1. INTRODUCTION

Hydrogen is a promising energy carrier that can be used to generate electricity in fuel cells without pollution.[1,2] However, to implement this fuel-cell-based hydrogen economy, practical solutions to controlled storage and release of hydrogen are essential.[2,3] Presently, hydrogen storage has been achieved by compressing the gas at high pressures, liquefying it at low temperatures, and storing it in the form of chemical/metal hydrides. However, all these methods suffer from a loss of hydrogen, safety issues, and low energy densities.[4,5]

Recently, formic acid has been suggested as a suitable material for hydrogen storage.[6,7] It contains 4.4 wt % of hydrogen with a volumetric capacity of 53.4 g/L at standard temperature and pressure (STP). Although its hydrogen content falls short of the milestones set by the U.S. Department of Energy for 2010 (5.5 wt %), its volumetric capacity surpasses that of most other storage materials used today.[6] Hydrogen stored in formic acid can be released on demand by decomposing formic acid into H_2 and CO_2.[8] If formic acid can be produced via CO_2 hydrogenation, a carbon-neutral hydrogen storage cycle can be achieved.[9,10] However, to develop formic acid as a hydrogen storage material, we first must find catalyst materials that can actively decompose formic acid to H_2 and CO_2.

Previous studies have shown that some precious metals are highly active for formic acid decomposition.[11,12] For example, Solymosi and co-workers[13] investigated formic acid decomposition over a range of monometallic catalysts containing various precious metals (Ir, Pd, Pt, Ru, or Rh supported on carbon) at 423 K. All their catalysts showed promising activities, to various extents. When the performance of different catalysts was compared, the activity trends of Ir ≈ Pt ≈ Pd > Ru > Rh were observed. However, these trends may not reflect the intrinsic catalytic properties of the precious metals, because the metal dispersion of the catalysts was different, ranging from 5.6% to 26.1%.

For direct applications in fuel cells, formic acid needs to be decomposed via dehydrogenation ($HCOOH \rightarrow H_2 + CO_2$) rather than via dehydration ($HCOOH \rightarrow H_2O + CO$) such that virtually CO-free hydrogen is produced. Many researchers have tried to achieve this by adding secondary metals to some precious metals. The improvements in hydrogen selectivity were particularly significant for Pd–Au[14,15] and Pd–Ag[16,17] catalysts, which produced H_2 with <100 ppm CO under ambient conditions. However, these catalysts are heavily based on expensive elements, and we must find alternative catalyst materials that are not only active and selective for formic acid dehydrogenation but also economically viable.

In this study, a theoretical analysis was used to identify alternative catalyst materials that can be used to decompose

Received: August 13, 2013
Revised: February 13, 2014
Published: March 13, 2014

 © 2014 American Chemical Society dx.doi.org/10.1021/cs400664z | ACS Catal. 2014, 4, 1226–1233

formic acid into H_2 and CO_2 under ambient conditions. Periodic density functional theory (DFT) calculations were employed to gain insights into the energetics of formic acid decomposition on Ag, Cu, Pd, Pt, and Rh surfaces.[18−21] A microkinetic model was also used to obtain the kinetics of formic acid decomposition over the transition-metal surfaces. The catalytic activities and selectivities of other transition-metal surfaces were then predicted using the "descriptors" found by scaling the calculated adsorption energies of the reaction species.[22,23] The variations in catalytic activity and selectivity from one metal surface to the next were finally compared to several experimental observations.

2. COMPUTATIONAL METHODS

DFT calculations were performed using the Dacapo code,[24] which implements plane waves to describe the valence electrons. Vanderbilt ultrasoft pseudo-potentials[25] were used to represent the ionic cores, and the RPBE functional[26] was used to describe the exchange and correlation effects of the electrons. All calculations were carried out with a kinetic energy cutoff of 340 eV and a density energy cutoff of 500 eV. The self-consistent electron density was determined by iterative diagonalization of the Kohn−Sham Hamiltonian, with the occupation of the Kohn−Sham states being smeared according to a Fermi−Dirac distribution with a smearing factor of k_BT = 0.1 eV, and the Pulay mixing of the resulting electron densities.[27]

Face-centered cubic (FCC(111) and FCC(211)) surfaces were modeled by periodic super cells containing three (or in some cases, four) atomic layers in the direction perpendicular to the surfaces. A (3 × 3) super cell was used for (111) slab models, and a (1 × 3) super cell was used for (211) slab models. The vertical distance between the slab models was 12 Å. The topmost atomic layer of the three-atomic-layer slab model (or, in some cases, the top two layers of the four-atomic-layer slab model), together with the adsorbates, was allowed to relax whereas the remaining two atomic layers were fixed in their bulk positions. For all calculations, 4 × 4 × 1 Monkhorst−Pack k-point sampling[28] was used to model the first Brillouin zone. Convergence of the adsorption energy, with respect to the k-point sampling and slab thickness, has been confirmed (see Table S9 in the Supporting Information). The convergence criterion for structural optimization was a maximum force of 0.05 eV/Å per atom, i.e., the force on each individual atom was <0.05 eV/Å.[29]

The vibrational frequencies, which are needed to determine zero-point energies and entropies, were calculated in the harmonic normal-mode approximation. They were calculated for a single surface, i.e., Cu(211), and were assumed to be constant for all others. This approximation has been justified because the variations in zero-point energy and entropic contribution were small, compared to the variation in electronic energy (see Table S1 in the Supporting Information).[20] The transition states were determined using either the fixed bond-length method,[23] in which the distance between the involved atoms was increased until a first-order saddle point was reached, or the nudged elastic band (NEB) approach.[30]

Recently, it has been shown that the newly developed BEEF−van der Waals (BEEF−vdW) functional[31] yields a better description of CO_2 hydrogenation to methanol on Cu(211), compared to the RPBE functional.[32] According to the reference, the BEEF−vdW functional was more accurate than the RPBE functional because it could address the vdW interaction, in addition to chemical bond formation. Since many of the reaction species involved in CO_2 hydrogenation to methanol are also involved in formic acid decomposition, it would have been better to use the BEEF−vdW functional than the RPBE functional in this study as well.

Given that the RPBE functional was used in this study, however, we had to address the vdW interaction in addition to chemisorption by making an empirical correction to the RPBE-calculated adsorption energies. The vdW-correction scheme was established based on the changes in adsorption energy observed for a single surface, i.e., Cu(211), when the RPBE functional was replaced with the BEEF−vdW functional in DFT calculations (see Table S10 in the Supporting Information). This manner of addressing the vdW interaction, i.e., independent of the catalyst surface, is only to a first approximation for surfaces other than Cu(211). However, it has been shown to be valid as the vdW-correction of the RPBE-calculated adsorption energies resulted in better agreement with experiments, compared to the case without the vdW-correction (see Tables S12 and S13, as well as Figure S2, in the Supporting Information).

We finally note here that the total energies of gas-phase molecules were corrected using the procedures described in our previous work.[32,33] This had to be done to ensure a good description of the energetics of the overall reactions.

3. RESULTS AND DISCUSSION

Scheme 1 shows the mechanism of formic acid decomposition considered in this study. Formic acid decomposition was

Scheme 1. The Reaction Mechanism of Formic Acid Decomposition[a]

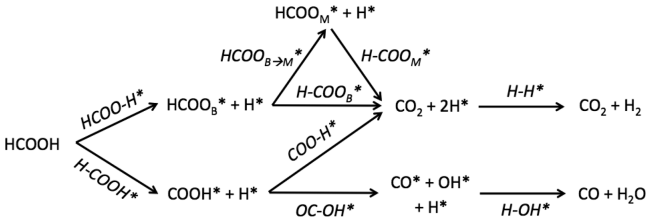

[a]Reaction species shown in *italic font* are the transition states, and those marked with an asterisk (*) are the reaction intermediates adsorbed on the surface.

initiated by activating either the O−H or C−H bond of the HCOOH to form formate (HCOO*) or carboxyl (COOH*) species on the surface. Activating the C−O bond of HCOOH to form formyl (CHO*) species on the surface was excluded from the mechanism, because it can be regarded as being energetically unfavorable, compared to activating either the O−H or C−H bond of HCOOH.[34−36] Bidentate formate ($HCOO_B$*), in which both oxygen atoms bind to the substrate, was found to be more stable than the monodentate formate ($HCOO_M$*), in which one oxygen atom binds to the substrate. For COOH* that binds to the substrate through the carbon atom, *trans*-COOH* was found to be more stable than *cis*-COOH*. Three different reaction pathways to form CO_2 were considered: one via C−H bond cleavage of $HCOO_B$*; one via C−H bond cleavage of $HCOO_M$* that has been formed by decoordination of $HCOO_B$*; and the other via O−H bond cleavage of *trans*-COOH*. On the other hand, there was only one reaction pathway to form CO*, which was via C−O bond

dx.doi.org/10.1021/cs400664z | ACS Catal. 2014, 4, 1226−1233

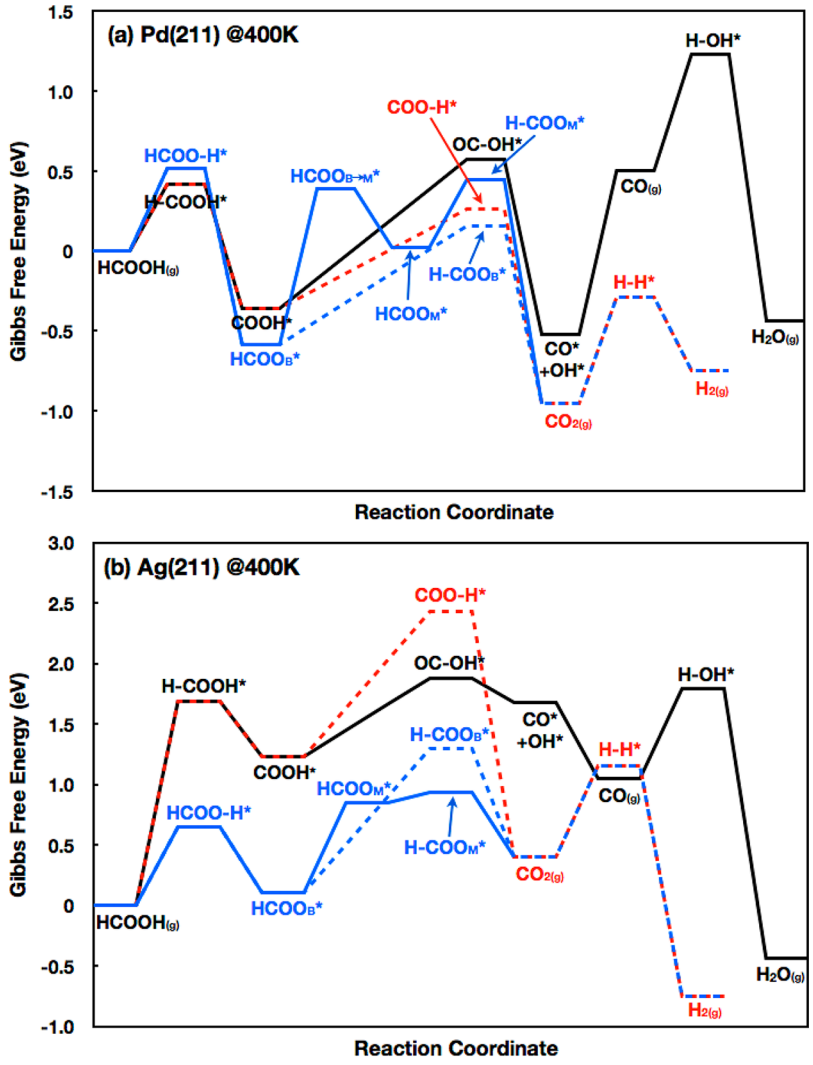

Figure 1. Gibbs energy diagram for formic acid decomposition on (a) Pd(211) and (b) Ag(211), calculated using the RPBE functional. All energies were vdW-corrected and were taken relative to the energy of formic acid in the gas phase. Species marked with an asterisk (*) are adsorbed on the surface. The H−COO_B*, H−COO_M*, and COO−H* pathways for formic acid dehydrogenation are depicted by the dashed blue line, the solid blue line, and the dashed red line, respectively, whereas the OC−OH* pathway for formic acid dehydration is depicted as a solid black line. Gibbs free energies were calculated using $\Delta G = \Delta E_{ads} + \Delta E_{ZPE} - T\Delta S$ (T = 400 K), where ΔE_{ads}, ΔE_{ZPE}, and ΔS represent the changes in adsorption energy, zero-point energy, and entropy, respectively.

cleavage of COOH*. The pathway of forming CO* from HCOO* was not considered because it requires simultaneous cleaving of C−H and C−O bonds of HCOO*. In summary, four different reaction pathways were considered for formic acid decomposition: H−COO_B*, H−COO_M*, and COO-H* pathways, which produced CO_2 and H_2 (dehydrogenation), and the OC−OH* pathway, which produced CO and H_2O (dehydration). The mechanistic choices we made here are in fair agreement with those made by others.[37−39] To help the reader visualize the reaction pathways, structural information about the transition states is provided in Tables S16 and S17 in the Supporting Information.

The RPBE functional was used to calculate the energetics of different reaction pathways for formic acid decomposition on five stepped surfaces (i.e., Ag(211), Cu(211), Pd(211), Pt(211), and Rh(211)) and three close-packed surfaces (i.e., Cu(111), Pd(111), and Pt(111)). All calculation results are shown in Tables S1−S8 in the Supporting Information. Here, we show the energetics for Pd(211) and Ag(211) in Figures 1a and 1b, respectively. A comparison between the two figures indicates that Pd(211) has relatively low free-energy barriers, compared to Ag(211). This agrees with previous experiments that Pd catalysts are highly active for formic acid decomposition.[13] Interestingly, dehydrogenation was preferred to dehydration on all of the surfaces that we investigated, although the minimum energy pathway (MEP) varied, depending on the surface. The MEP occurred via COO−H* on Pd(211), Pt(211), Pd(111), and Pt(111), via H−COO_M* on Ag(211), Cu(211), and Rh(211), and via H−COO_B* on Cu(111). However, we should be careful not to conclude that the reaction always proceeds via the MEP, because the surface can be poisoned by the strongly bound intermediates that are formed along the MEP. Comparing the energetics of different reaction pathways does not provide information about the availability of free adsorption sites that are required to decompose the surface species. This information can only be obtained by a detailed microkinetic analysis.

We extended the study to other transition-metal surfaces by establishing trends in the calculated adsorption energies of the reaction species from one metal surface to another. This was

dx.doi.org/10.1021/cs400664z | ACS Catal. 2014, 4, 1226−1233

done using the adsorption energy scaling law that can be stated as follows: the adsorption energy of an adsorbate that binds to a surface through atom A correlates linearly with the adsorption energy of atom A on the surface.[40,41] In the case of formic acid decomposition, all reaction species except hydrogen bind to the surface through the carbon atom and/or the oxygen atom. Accordingly, we can scale their adsorption energies with the carbon and/or oxygen adsorption energies. For hydrogen, we can exploit the fact that hydrogen adsorption energies correlate well with carbon adsorption energies.[20] In summary, we can scale all adsorption energies of the reaction species involved in formic acid decomposition with carbon and/or oxygen adsorption energies. In this study, however, we decided to scale them with CO and/or OH adsorption energies (ΔE_{CO} and/or ΔE_{OH}), because both CO and OH are already involved in the reaction mechanism, and their adsorption energies are known to correlate well with carbon and oxygen adsorption energies, respectively.[23,42]

Figure 2 shows the scaling relations obtained when we scaled the adsorption energies of the reaction species adsorbed on Ag(211), Cu(211), Pd(211), Pt(211), Rh(211), Cu(111), Pd(111), and Pt(111) with ΔE_{CO} and/or ΔE_{OH}. Interestingly, the scaling relations obtained for individual species were found to be approximately independent of whether the surface structure is (211) or (111). This coincides with our previous finding that the transition-state scaling relations are very similar over the stepped and close-packed surfaces for AH_x dehydrogenation (A = C, N, or O).[42] However, it is still not quite intuitive to find that the scaling relations are independent of the surface structure for not just the transition states but also the reaction intermediates, because geometric effects cannot be completely absent for some adsorbates. Nevertheless, for the sake of simplicity, we intended to use the same scaling relations to estimate the adsorption energies of the reaction species adsorbed on other (211) and (111) surfaces by obtaining two independent descriptors per surface: ΔE_{CO} and ΔE_{OH}.

The kinetics of different reaction pathways for formic acid decomposition were obtained from the self-consistent steady-state solution to a microkinetic model that was built to include all reaction steps shown in Scheme 1. The reaction rates of the elementary reactions were described based on the mean field approximation, and harmonic transition state theory was used to derive the prefactors of the Arrhenius-type relations (see the Supporting Information for details).[20,43,44] The reaction conditions used in the microkinetic model were T = 400 K and P = 1 bar with ~1% approach to equilibrium toward H_2 and CO_2 (97% HCOOH, 1% H_2, 1% CO_2, 1% H_2O, and 100 ppm CO). Finally, we have accounted for the overbinding of CO in DFT by adding 0.25 eV to the scaling relation obtained for CO when this was incorporated in the microkinetic model.[29] In connection with the scaling relations, our microkinetic model calculates the turnover frequencies (TOFs) for formic acid decomposition as functions of ΔE_{CO} and ΔE_{OH}.

Figure 3a shows the logarithms of the calculated TOFs for H_2 + CO_2 production from formic acid decomposition over various transition-metal surfaces. Volcano-shaped relations were obtained when the logarithms of the TOFs were mapped as functions of ΔE_{CO} and ΔE_{OH}. As expected from previous experimental studies,[13] the five precious metals (Ir, Pd, Pt, Ru, and Rh) were calculated to show high rates for hydrogen production. However, we have found that these precious metals are not at the top of the activity volcano, and there can be other materials that exhibit even higher activity if they were to bind CO and/or OH slightly weaker than the precious metals. We will now compare the catalytic activity trends of formic acid decomposition obtained from our analysis with other experimental observations reported in the literature.

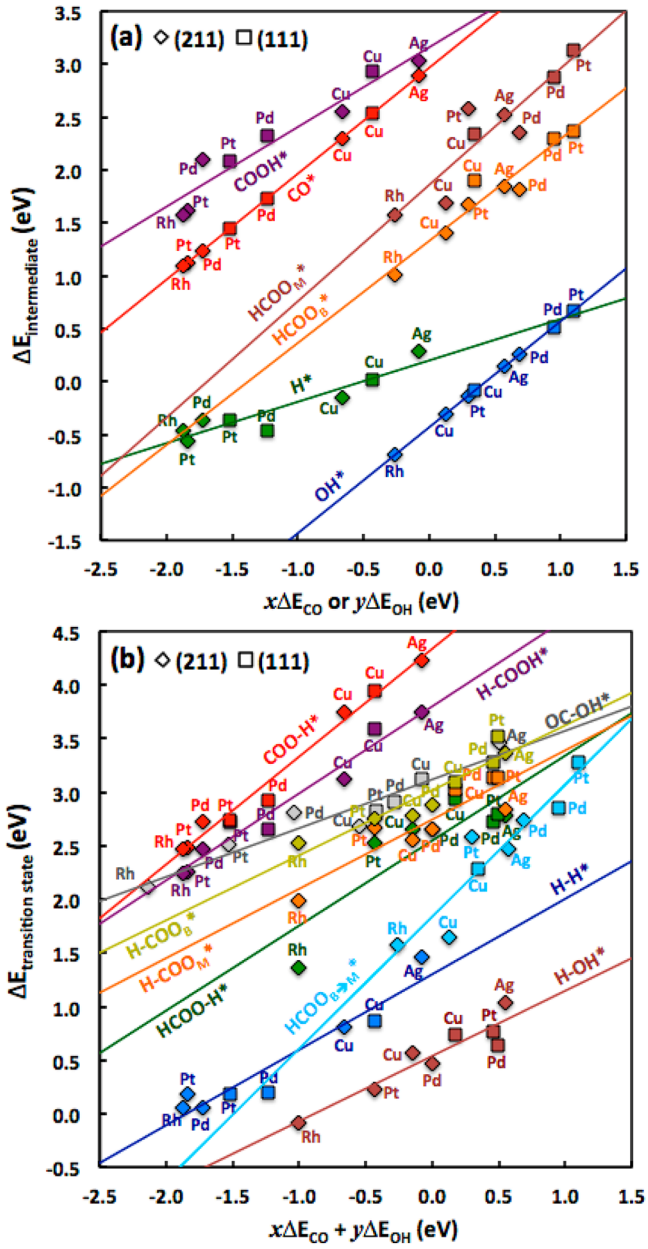

Figure 2. Scaling relations of vdW-corrected adsorption energies of the (a) reaction intermediates and the (b) transitions states adsorbed on their most stable sites. On Pd(111), however, CO adsorbed on the on-top site was used instead of CO adsorbed on the most stable site (see Table S4 in the Supporting Information). All vdW-corrected adsorption energies were taken relative to electronic energies of CH_4, H_2, and H_2O in the gas phase, and were plotted as functions of CO and/or OH adsorption energies (ΔE_{CO}, ΔE_{OH}) that were taken relative to electronic energies of CO, H_2, and H_2O in the gas phase without the vdW correction. Zero-point energies are not included. The solid lines were obtained by the best fits through the eight data points; the slopes and the intercepts of the fits as well as the values of x and y in the x-axes are given in Tables S14 and S15 in the Supporting Information.

dx.doi.org/10.1021/cs400664z | ACS Catal. 2014, 4, 1226−1233

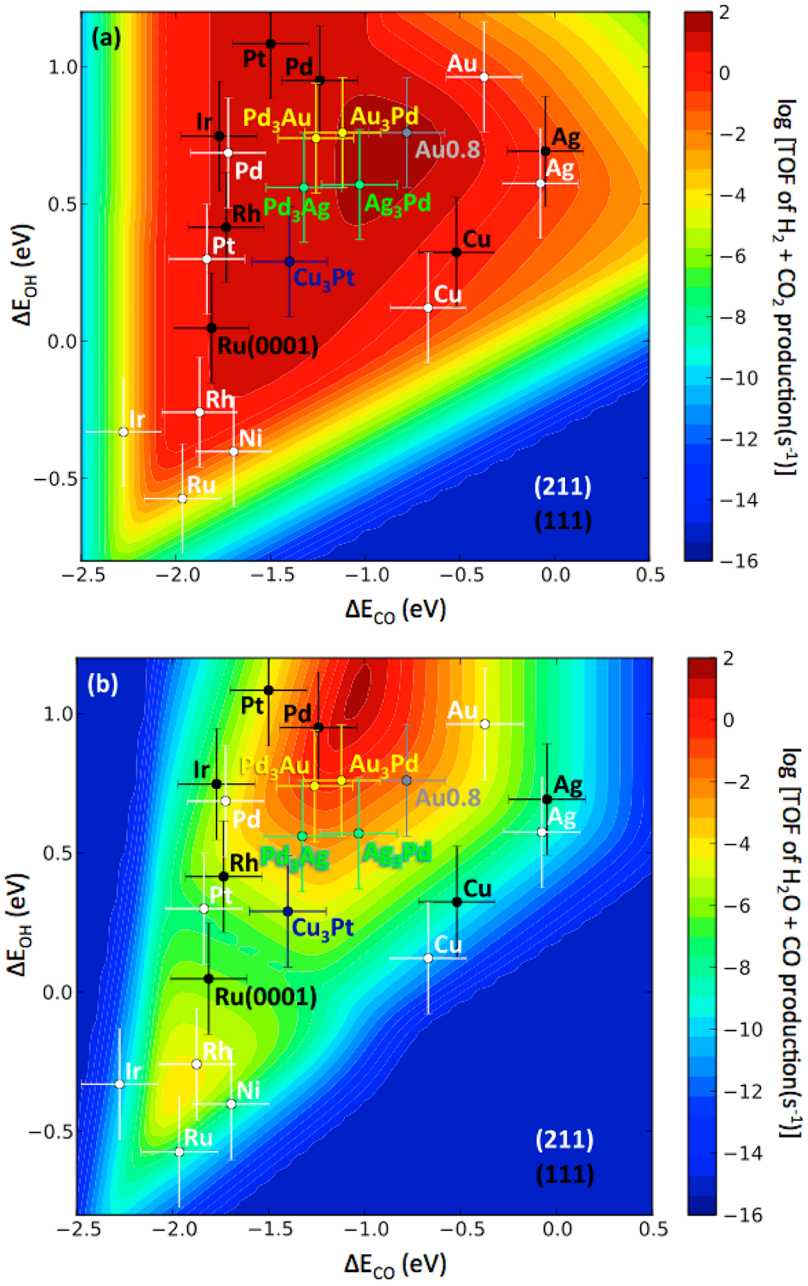

Figure 3. Theoretical activity volcanoes for (a) H_2 + CO_2 production and (b) H_2O + CO production from formic acid. The logarithms of the turnover frequencies (TOFs) were plotted as functions of CO and OH adsorption energies (ΔE_{CO} and ΔE_{OH}) that were taken relative to electronic energies of CO, H_2, and H_2O in the gas phase. The calculated ΔE_{CO} and ΔE_{OH} for the stepped and terrace sites of selected transition metals are depicted in white and black, respectively. The calculated ΔE_{CO} and ΔE_{OH} for the stepped site (AB step) of Pd−Au and Pd−Ag(211) alloys ($L1_2$-type A_3B ordering) are depicted in yellow and green, respectively. The calculated ΔE_{CO} and ΔE_{OH} for the terrace site of $Cu_3Pt(111)$ ($L1_2$-type A_3B ordering) are depicted in blue. The Au0.8 data point, which is depicted in gray, represents the calculated ΔE_{CO} and ΔE_{OH} for the (111)-type facet of a 13-atom gold cluster, the diameter of which is ∼0.8 nm. This data point was derived from the data presented in ref 46. We also note here that CO adsorbed on the on-top site was used as a descriptor for Pd(111) instead of CO adsorbed on the most stable site (see Table S4 in the Supporting Information). Finally, the error bars indicate an estimated error of 0.2 eV for ΔE_{CO} and ΔE_{OH}, compared to their experimental values.

Previously, Ojeda et al. showed that highly dispersed gold nanoparticles supported on Al_2O_3 can exhibit considerable formic acid decomposition activity.[45] The intrinsic catalytic activity of the Au nanoparticles began to exceed that of the Pt nanoparticles decreasing particle size. According to Figure 3a, however, Au(211) is calculated to be less active than Pt(211) and Pt(111), because it lies far out on the weak-binding side of the activity volcano. We attribute the enhanced catalytic activity of the gold nanoparticles to the quantum-size effect that is existent in small gold clusters (<2.7 nm).[46,47] For example, a gold cluster of diameter 0.8 nm was calculated to bind CO and OH far more strongly than Au(211),[46] which brings it very close to the top of the activity volcano.

Recently, highly dispersed Pd−Au[14,15] and Pd−Ag[16,17] binary alloys were demonstrated to be extremely active for formic acid decomposition. We calculated ΔE_{CO} and ΔE_{OH} for the stepped sites of Pd−Au and Pd−Ag binary alloys and found that these alloys are indeed at the top of the activity volcano. In

dx.doi.org/10.1021/cs400664z | ACS Catal. 2014, 4, 1226−1233

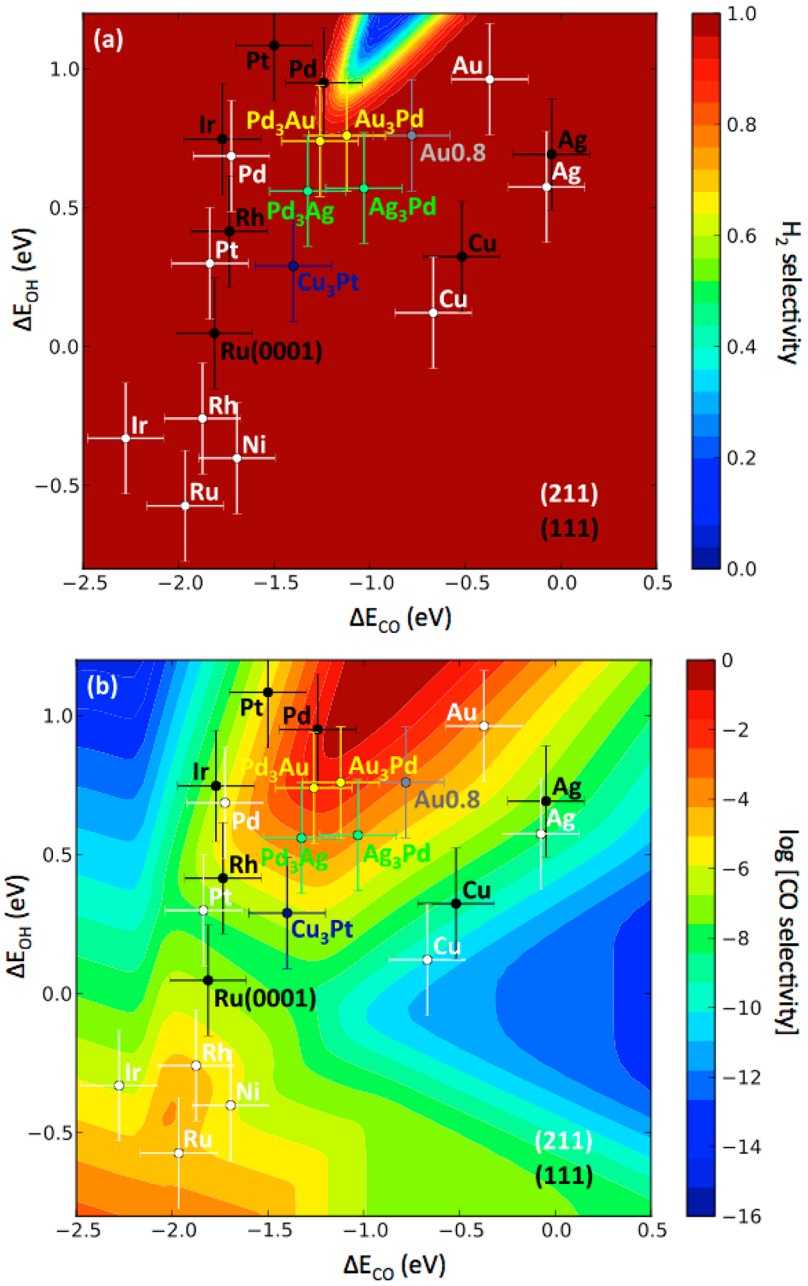

Figure 4. (a) Calculated H_2 selectivities and (b) logarithms of the calculated CO selectivities, as functions of ΔE_{CO} and ΔE_{OH} that were taken relative to electronic energies of CO, H_2 and H_2O in the gas phase. H_2 (or CO) selectivity is defined as the production rate of H_2 + CO_2 (or H_2O + CO) divided by the total rate of formic acid decomposition. The labels used in the figure are the same as those shown in the caption of Figure 3. The error bars indicate an estimated error of 0.2 eV for ΔE_{CO} and ΔE_{OH}, compared to their experimental values.

fact, the most active heterogeneous catalyst ever reported for formic acid decomposition was monodisperse 2.2 nm Pd–Ag alloy nanoparticles.[17] Interestingly, the calculated ΔE_{CO} and ΔE_{OH} for the Pd–Au and Pd–Ag binary alloys were found to be intermediate between those of Pd and Au (or Ag).[48−50] For example, ΔE_{CO} and ΔE_{OH} for $Pd_3Au(211)$ were interpolative of those for Pd(211) and Au(211). This interpolation concept of adsorption energy holds promise because we can now quickly look for potentially interesting alloy catalysts by initially carrying out a rough screening based on the adsorption energies for the elemental metals.

Figure 3b shows the logarithms of the calculated TOFs for H_2O + CO production from formic acid decomposition, which were also mapped as functions of ΔE_{CO} and ΔE_{OH}. A comparison between Figures 3a and 3b reveals that the dehydrogenation reaction is faster than the dehydration reaction on almost all transition-metal surfaces, by several orders of magnitude. Accordingly, hydrogen selectivities were calculated to be almost 1 for most of the surfaces, as shown in Figure 4a. For direct applications in fuel cells, however, the CO concentration in hydrogen feedstock must be reduced well below 100 ppm.[51] To take a closer look at the variations in the CO concentration from one metal surface to another, we calculated the logarithms of CO selectivities as functions of ΔE_{CO} and ΔE_{OH}, and the results are shown in Figure 4b. A gold cluster 0.8 nm in diameter, and the stepped sites of the Pd–Au and Pd–Ag binary alloys were all calculated to produce >100 ppm CO (CO selectivity = 10^{-4}) under the reaction conditions

dx.doi.org/10.1021/cs400664z | ACS Catal. 2014, 4, 1226−1233

used in our microkinetic model. It would be desirable to find alternative catalyst materials that are more hydrogen-selective but less expensive than the Au clusters or the Pd−Au, Pd−Ag alloys.

The interpolation concept of adsorption energy was used to look for other potentially interesting alloy catalysts, but only within the set of data obtained thus far. Pt−Cu alloys have attracted our attention, because the descriptor space between Pt(211) and Cu(211) represents the region of low CO selectivity in Figure 4b, and the region of high catalytic activity in Figure 3a. We thus calculated ΔE_{CO} and ΔE_{OH} for the terrace site of Cu_3Pt, and we found that our model estimates this alloy to produce ≪100 ppm CO (see Figure 4) while being as active as the conventional precious metals (see Figure 3a). The Cu_3Pt alloy is particularly interesting, because it is calculated to be thermodynamically stable, and it is not heavily dependent on the rare-earth elements. While the Cu_3Pt alloy is a first example of a possible lead for a new material, we believe that more candidates can be found using the methodology presented in this study.

4. CONCLUSIONS

A theoretical analysis was conducted to investigate formic acid decomposition with relevance to hydrogen storage. The reaction energetics of formic acid decomposition were obtained based on the vdW-corrected adsorption energies of the reaction species adsorbed on five stepped surfaces (i.e., Ag(211), Cu(211), Pd(211), Pt(211), and Rh(211)) and three close-packed surfaces (i.e., Cu(111), Pd(111), and Pt(111)). Formic acid decomposition was found to proceed via dehydrogenation rather than dehydration, although the minimum energy pathway varied, depending on the catalyst surface. The study was also extended to other transition-metal surfaces by utilizing the scaling relations that correlated the adsorption energies of the reaction species with two independent descriptors: ΔE_{CO} and ΔE_{OH}. By incorporating the scaling relations in a microkinetic model, two-dimensional volcano plots were constructed, which showed the turnover frequencies (TOFs) for $H_2 + CO_2$ production and $H_2O + CO$ production as functions of the two descriptors. The catalytic activity trends obtained in this study were consistent with many experimental observations reported in the literature. We also constructed volcano plots showing H_2 selectivities and CO selectivities as functions of the two descriptors, which were conveniently used to search for new alloy catalysts of extremely low CO selectivity, based on the interpolation concept of adsorption energy. As a result, the Cu_3Pt alloy was identified to be one of the potentially interesting catalyst materials.

■ ASSOCIATED CONTENT

Supporting Information

Additional information about the calculation results, convergence with respect to *k*-point sampling density and slab thickness, vdW correction to the RPBE-calculated adsorption energies, justification for the vdW correction, scaling relations, and the microkinetic model. This material is available free of charge via the Internet at http://pubs.acs.org.

■ AUTHOR INFORMATION

Corresponding Author

*E-mail: studt@slac.stanford.edu.

Notes

The authors declare no competing financial interest.

■ ACKNOWLEDGMENTS

We gratefully acknowledge the support from the U.S. Department of Energy, Office of Basic Energy Sciences to the SUNCAT Center for Interface Science and Catalysis. J.S.Y. would like to thank the U.S. Department of State for funding his Ph.D. studies at Stanford University through the International Fulbright Science & Technology Award program. Last, but not least, we thank Dr. Heine A. Hansen for sharing his CO and OH adsorption energies on the Pd−Au and Pd−Ag alloys, and Dr. Adam C. Lausche for sharing his CO and OH adsorption energies on the Cu_3Pt alloy.

■ REFERENCES

(1) Turner, J. A. *Science* **2004**, *305*, 972−974.
(2) Schlapbach, L.; Züttel, A. *Nature* **2001**, *414*, 353−358.
(3) Navarro, R. M.; Peña, M. A.; Fierro, J. L. G. *Chem. Rev.* **2007**, *107*, 3952−3991.
(4) Felderhoff, M.; Weidenthaler, C.; von Helmolt, R.; Eberle, U. *Phys. Chem. Chem. Phys.* **2007**, *9*, 2643−2653.
(5) Enthaler, S.; von Langermann, J.; Schmidt, T. *Energy Environ. Sci.* **2010**, *3*, 1207−1217.
(6) Grasemann, M.; Laurenczy, G. *Energy Environ. Sci.* **2012**, *5*, 8171−8181.
(7) Boddien, A.; Gärtner, F.; Federsel, C.; Sponholz, P.; Mellmann, D.; Jackstell, R.; Junge, H.; Beller, M. *Angew. Chem., Int. Ed.* **2011**, *50*, 6411−6414.
(8) Bi, Q.-Y.; Du, X.-L.; Liu, Y.-M.; Cao, Y.; He, H.-Y.; Fan, K.-N. *J. Am. Chem. Soc.* **2012**, *134*, 8926−8933.
(9) Boddien, A.; Junge, H. *Nat. Nanotechnol.* **2011**, *6*, 265−266.
(10) Hull, J. F.; Himeda, Y.; Wang, W.-H.; Hashiguchi, B.; Periana, R.; Szalda, D. J.; Muckerman, J. T.; Fujita, E. *Nat. Chem.* **2012**, *4*, 383−388.
(11) Tang, Y.; Roberts, C. A.; Perkins, R.; Wachs, I. E. *Revisiting Formic Acid Decomposition on Bulk Metallic Catalysts*. Presented at the *23rd North American Catalysis Society Meeting*, Louisville, KY, June 2−7, 2013, Paper No. O-Tu-Seg-8.
(12) Bulushev, D. A.; Beloshapkin, S.; Ross, J. R. H. *Catal. Today* **2010**, *154*, 7−12.
(13) Solymosi, F.; Koós, Á.; Liliom, N.; Ugrai, I. *J. Catal.* **2011**, *279*, 213−219.
(14) Huang, Y.; Zhou, X.; Yin, M.; Liu, C.; Xing, W. *Chem. Mater.* **2010**, *22*, 5122−5128.
(15) Zhou, X.; Huang, Y.; Xing, W.; Liu, C.; Liao, J.; Lu, T. *Chem. Commun.* **2008**, *30*, 3540−3542.
(16) Tedsree, K.; Li, T.; Jones, S.; Chan, C. W. A.; Bagot, P. A. J.; Marquis, E. A.; Smith, G. D. W.; Yu, K. M. K.; Tsang, S. C. E. *Nat. Nanotechnol.* **2011**, *6*, 302−307.
(17) Zhang, S.; Metin, O.; Su, D.; Sun, S. *Angew. Chem., Int. Ed.* **2013**, *52*, 1−5.
(18) Studt, F.; Abild-Pedersen, F.; Bligaard, T.; Sørensen, R. Z.; Christensen, C. H.; Nørskov, J. K. *Science* **2008**, *320*, 1320−1322.
(19) Behrens, M.; Studt, F.; Kasatkin, I.; Kühl, S.; Hävecker, M.; Abild-Pedersen, F.; Zander, S.; Girgsdies, F.; Kurr, P.; Kniep, B.-L.; Tovar, M.; Fischer, R. W.; Nørskov, J. K.; Schlögl, R. *Science* **2012**, *336*, 893−897.
(20) Jones, G.; Jakobsen, J. G.; Shim, S. S.; Kleis, J.; Andersson, M. P.; Rossmeisl, J.; Abild-Pedersen, F.; Bligaard, T.; Helveg, S.; Hinnemann, B.; Rostrup-Nielsen, J. R.; Chorkendorff, I.; Sehested, J.; Nørskov, J. K. *J. Catal.* **2008**, *259*, 147−160.
(21) Greeley, J.; Mavrikakis, M. *Nat. Mater.* **2004**, *3*, 810−815.
(22) Grabow, L. C.; Studt, F.; Abild-Pedersen, F.; Petzold, V.; Kleis, J.; Bligaard, T.; Nørskov, J. K. *Angew. Chem., Int. Ed.* **2011**, *50*, 4601−4605.

(23) Studt, F.; Abild-Pedersen, F.; Wu, Q.; Jensen, A. D.; Temel, B.; Grunwaldt, J.-D.; Nørskov, J. K. *J. Catal.* **2012**, *293*, 51−60.
(24) Bahn, S. R.; Jacobsen, K. W. *Comput. Sci. Eng.* **2002**, *4*, 56−66.
(25) Laasonen, K.; Car, R.; Lee, C.; Vanderbilt, D. *Phys. Rev. B* **1991**, *43*, 6796−6799.
(26) Hammer, B.; Hansen, L. B.; Nørskov, J. K. *Phys. Rev. B* **1999**, *59*, 7413−7421.
(27) Kresse, G.; Furthmüller, J. *Comput. Mater. Sci.* **1996**, *6*, 15−50.
(28) Chadi, D. J. *Phys. Rev. B* **1977**, *16*, 1746−1747.
(29) Abild-Pedersen, F.; Andersson, M. P. *Surf. Sci.* **2007**, *601*, 1747−1753.
(30) Jacobsen, K. W.; Jonson, H.; Mills, G. Classical and Quantum Dynamics in Condensed Phase Simulations. In *Proceedings of the International School of Physics*, Lerici, Italy, July 7−18, 1997; Berne, B. J., Coker, D. F., Ciccotti, G., Eds.; World Scientific Publishing Company: Singapore, 1998.
(31) Wellendorff, J.; Lundgaard, K. T.; Møgelhøj, A.; Petzold, V.; Landis, D. D.; Nørskov, J. K.; Bligaard, T.; Jacobsen, K. W. *Phys. Rev. B* **2012**, *85*, 235149.
(32) Studt, F.; Abild-Pedersen, F.; Varley, J. B.; Nørskov, J. K. *Catal. Lett.* **2013**, *143*, 71−73.
(33) Peterson, A. A.; Abild-Pedersen, F.; Studt, F.; Rossmeisl, J.; Nørskov, J. K. *Energy Environ. Sci.* **2010**, *3*, 1311−1315.
(34) Li, S. J.; Zhou, X.; Tian, W. Q. *J. Phys. Chem. A* **2012**, *116*, 11745−11752.
(35) Zhang, R.; Liu, H.; Wang, B.; Ling, L. *J. Phys. Chem. C* **2012**, *116*, 22266−22280.
(36) Duan, S.; Ji, Y.-F.; Fang, P.-P.; Chen, Y.-X.; Xu, X.; Luo, Y.; Tian, Z.-Q. *Phys. Chem. Chem. Phys.* **2013**, *15*, 4625−4633.
(37) Grabow, L. C.; Gokhale, A. A.; Evans, S. T.; Dumesic, J. A.; Mavrikakis, M. *J. Phys. Chem. C* **2008**, *112*, 4608−4617.
(38) Grabow, L. C.; Mavrikakis, M. *ACS Catal.* **2011**, *1*, 365−384.
(39) Gokhale, A. A.; Dumesic, J. A.; Mavrikakis, M. *J. Am. Chem. Soc.* **2008**, *130*, 1402−1414.
(40) Abild-Pedersen, F.; Greeley, J.; Studt, F.; Rossmeisl, J.; Munter, T. R.; Moses, P. G.; Skúlason, E.; Bligaard, T.; Nørskov, J. K. *Phys. Rev. Lett.* **2007**, *99*, 016105.
(41) Jones, G.; Studt, F.; Abild-Pedersen, F.; Nørskov, J. K.; Bligaard, T. *Chem. Eng. Sci.* **2011**, *66*, 6318−6323.
(42) Wang, S.; Petzold, V.; Tripkovic, V.; Kleis, J.; Howalt, J. G.; Skúlason, E.; Fernández, E. M.; Hvolbæk, B.; Jones, G.; Toftelund, A.; Falsig, H.; Björketun, M.; Studt, F.; Abild-Pedersen, F.; Rossmeisl, J.; Nørskov, J. K.; Bligaard, T. *Phys. Chem. Chem. Phys.* **2011**, *13*, 20760−20765.
(43) Nilsson, A.; Pettersson, L. G. M.; Nørskov, J. *Chemical Bonding at Surfaces and Interfaces*; Elsevier Science: Amsterdam, 2011; p 532.
(44) Lausche, A. C.; Hummelshøj, J. S.; Abild-Pedersen, F.; Studt, F.; Nørskov, J. K. *J. Catal.* **2012**, *291*, 133−137.
(45) Ojeda, M.; Iglesia, E. *Angew. Chem., Int. Ed.* **2009**, *121*, 4894−4897.
(46) Kleis, J.; Greeley, J.; Romero, N. A.; Morozov, V. A.; Falsig, H.; Larsen, A. H.; Lu, J.; Mortensen, J. J.; Dułak, M.; Thygesen, K. S.; Nørskov, J. K.; Jacobsen, K. W. *Catal. Lett.* **2011**, *141*, 1067−1071.
(47) Li, L.; Larsen, A. H.; Romero, N. A.; Morozov, V. A.; Glinsvad, C.; Abild-Pedersen, F.; Greeley, J.; Jacobsen, K. W.; Nørskov, J. K. *J. Phys. Chem. Lett.* **2013**, *4*, 222−226.
(48) Nørskov, J. K.; Bligaard, T.; Rossmeisl, J.; Christensen, C. H. *Nat. Chem.* **2009**, *1*, 37−46.
(49) Hansgen, D. A.; Vlachos, D. G.; Chen, J. G. *Nat. Chem.* **2010**, *2*, 484−489.
(50) Jacobsen, C. J.; Dahl, S.; Clausen, B. S.; Bahn, S.; Logadottir, A.; Nørskov, J. K. *J. Am. Chem. Soc.* **2001**, *123*, 8404−8405.
(51) Yoo, J. S.; Kim, H.; Joh, H.; Kim, H. T.; Moon, S. H. *Int. J. Hydrogen Energy* **2011**, *36*, 1930−1938.